






K-Edge Structure in Shock-Compressed Chlorinated Parylene

David Bailie ¹ , Steven White ¹, Rachael Irwin ¹, Cormac Hyland ¹ , Richard Warwick ¹, Brendan Kettle ^{1,2} , Nicole Breslin ¹, Simon N. Bland ², David J. Chapman ², Stuart P. D. Mangles ² , Rory A. Baggot ², Eleanor R. Tubman ² and David Riley ^{1,*} 

¹ Centre for Light-Matter Interaction, School of Mathematics and Physics, Queen's University Belfast, University Road, Belfast BT7 1NN, UK; swhite06@qub.ac.uk (S.W.); rirwin11@qub.ac.uk (R.I.)

² Plasma Physics Group, Blackett Laboratory, Imperial College, London SW7 2BZ, UK; david.chapman@eng.ox.ac.uk (D.J.C.)

* Correspondence: d.riley@qub.ac.uk

Abstract: We have carried out a series of experiments to measure the Cl K-absorption edge for shock-compressed samples of chlorinated parylene. Colliding shocks allowed us to compress samples up to four times the initial density with temperatures up to 10 eV. Red shifts in the edge of about 10 eV have been measured. We have compared the measured shifts to analytical modelling using the Stewart–Pyatt model and adaptations of it, combined with estimates of density and temperature based on hydrodynamic modelling. Modelling of the edge position using density functional theory molecular dynamics (DFT-MD) was also used and it was found that good agreement was only achieved when the DFT simulations assumed conditions of lower temperature and slightly higher density than indicated by hydrodynamic simulations using a tabular equation of state.

Keywords: ionization potential depression; continuum lowering; X-ray spectroscopy

PACS: 52.38.Ph; 52.38.Dx; 52.70.La



Citation: Bailie, D.; White, S.; Irwin, R.; Hyland, C.; Warwick, R.; Kettle, B.; Breslin, N.; Bland, S.N.; Chapman, D.J.; Mangles, S.P.D.; et al. K-Edge Structure in Shock-Compressed Chlorinated Parylene. *Atoms* **2023**, *11*, 135. <https://doi.org/10.3390/atoms11100135>

Academic Editor: Frank B. Rosmej

Received: 17 August 2023

Revised: 22 September 2023

Accepted: 13 October 2023

Published: 18 October 2023



Copyright: © 2023 by the authors. Licensee MDPI, Basel, Switzerland. This article is an open access article distributed under the terms and conditions of the Creative Commons Attribution (CC BY) license (<https://creativecommons.org/licenses/by/4.0/>).

1. Introduction

It is commonly acknowledged in the literature relating to warm dense matter, e.g., [1–3], that it is not only a challenging state of matter to describe theoretically, but that it is also challenging to diagnose experimentally. The theoretical challenge arises from the presence of strong inter-particle correlation, partial ionisation and partial degeneracy. The diagnostic challenges include the fact that the extreme conditions of warm dense matter generally require dynamic methods of sample generation, often on timescales of nanoseconds or shorter. In addition, the density is too high for optical emission to escape, except from the surface of the sample, where the plasma temperature and density may not reflect the interior values. Further, the sample is usually too cold for X-ray emission. For this reason, there has been a concerted effort over the last couple of decades to develop X-ray probe diagnostics, such as X-ray Thomson scattering and K-edge spectroscopy, including techniques such as X-ray absorption near edge structure (XANES), which looks in the region near to the K-edge, and extended X-ray absorption fine structure (EXAFS), looking at oscillations in absorption further from the edge. Both are influenced by the environment of the species whose edge is explored. At higher temperatures, the detailed edge structure present in XANES and EXAFS tends to be washed out and the position of the edge and the slope become the features of interest. For this, the ionisation potential depression (IPD) is a key factor.

Ionisation potential depression and pressure ionisation are important processes in shock-compressed warm dense matter (WDM) where the electronic structure of the ions plays a key role in the bulk properties of the matter. In the past, K-edge shift experiments [4–6] have been modelled, typically by using an ion-sphere approach to IPD. An important

experimental challenge in such experiments is that the red-shift of the edge caused by IPD is mostly balanced by a blue-shift due to ionisation of the sample with additional, usually smaller shifts due to changes in the degeneracy of the free electrons. This means that although the IPD may be of the order of 100 eV, the actual K-edge shifts are generally only a few eV. Other challenges in modelling such experiments with an analytical model include the fact that both the ionisation blue-shift and the IPD depend on defining the average ionisation, which in dense plasmas can be ill defined, with some electrons having negative energy, i.e., bound, but being delocalised as in a metal.

In the last decade, the subject of IPD in dense plasmas has seen a resurgence of interest [7–10]. This has been driven by the fact that, in experiments with the Linear Coherent Light Source (LCLS) X-ray laser facility [7], application of the long accepted Stewart–Pyatt model [11] failed to explain the emission data observed from solid density Al heated with an X-ray pulse. Instead, an older approach by Ecker and Kröll [12] provided a better fit. However, a later experiment by Hoarty et al. [8] indicated that it was the Stewart–Pyatt model and not the Ecker–Kröll model that could explain the observations of He-like Al lines in an experiment where shock-compressed Al was heated by fast electrons from an intense short pulse laser interaction with the target. The potential reasons for these apparently divergent findings were discussed in detail by Crowley [9] and Iglesias [10] and include the effect of electron polarisation and the interaction energy of photoionised electrons with the plasma medium.

The Stewart–Pyatt and Ecker–Kröll models have been known for several decades. More recently, it has been possible to carry out relatively fast molecular dynamics simulations using density functional theory (DFT-MD). This has the advantages that the effect of ion–ion correlations on the local field are accounted for and we do not need to make a distinction between bound and free electrons, which, as noted above, can be ambiguous.

In this paper, we present the results of an experiment to measure the K-edge shift in shock-compressed and heated samples. The targets consisted of 20 μm of parylene-C ($\text{C}_8\text{H}_7\text{Cl}$) sandwiched between two 20 μm layers of parylene-N (C_8H_8). By probing at different times relative to the shock drive, we can probe different density and temperature combinations.

2. Experiment

The experiment is shown schematically in Figure 1. The samples were compressed by colliding laser-driven shocks created with the VULCAN laser facility operating at 527 nm, with two opposing clusters of three beams. The beams were focussed with $f/10$ optics using phase plates that generated a flat-topped, 500 μm square focal spot. The pulses were temporally shaped to have a steep rise to $\sim 3.3 \times 10^{13} \text{ Wcm}^{-2}$ over ~ 250 ps followed by a roughly linear decline to $1.7 \times 10^{13} \text{ Wcm}^{-2}$ over ~ 1.5 ns and finally a steep drop to zero over 200 ps. The opposing clusters were simultaneously incident on the target to an accuracy of approximately 30 ps. The K-edge of the Cl was monitored by two X-ray back-light probes. These were generated by 200 ps Gaussian pulses (527 nm) focussed to 70–100 μm onto a thin Bi layer coated onto a CH support layer. The M-shell X-rays from the Bi passed through the target at 45° (thus, the back-light beams were orthogonal to each other) and the timing of the two probe beams was varied relative to the shock-driving beams. The jitter between the probe and shock drive was on the order of 100 ps, but timing fiducials, derived from beam leakage through mirrors, allowed us to monitor the relative timing to better than 30 ps. The spectra of the Bi around the Cl K-edge were recorded with two Si (111) CCD spectrometers with 13 μm square pixels. The back-lighters were placed 7 mm from the sample and this was 211 mm from the CCD plane. This means that, in the spectral direction, the total range of X-rays sampled passed through a section of the sample 0.44 mm high, less than the size of the flat-topped focal spot. The X-ray source size was monitored with a filtered pinhole camera and was less than 100 μm . This means that spatial resolution of the shocked region was possible. The spectral broadening of the

spectrometers was determined by a combination of the pixel size, source size and crystal resolution to be better than 1.5 eV.

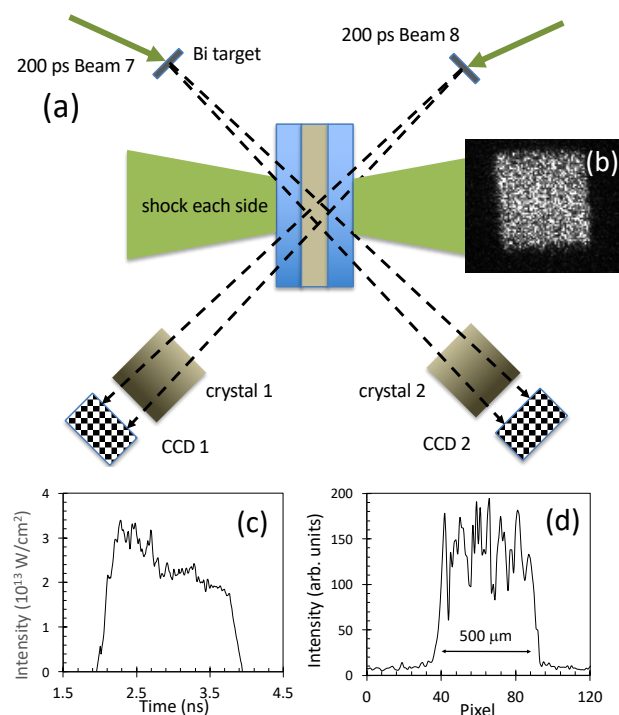


Figure 1. (a) Schematic of the experimental arrangement. The Bi targets were positioned 7 mm from the shock-compressed sample. The three targets were pre-aligned on a target alignment rig which ensured that the line of sight from back-lighter to the spectrometer passed through the shock-compressed region. (b) The inset shows an image of a typical beam intensity profile using the square phase plates. (c) Pulse history of the 527 nm optical drive laser. (d) A horizontal line-out, averaged over a line 10 pixels wide, of the beam spatial profile across the centre of the focal spot.

3. Results

In Figure 2a, we can see an example of a raw data shot. We can see the spatially resolved shock region where the K-edge is broader and shifted from the cold edge position. The darker region on the left was due to a razor edge placed at the entrance to the front of the spectrometer that blocked the direct back-lighter X-rays. This region contained fluorescence from the crystal. There is a penumbral region that, due to the larger size and closer position of the shocked region compared to the back-lighter, contains emission from the shocked plasma and allows background subtraction to be carried out. Calibration shots with just the Bi and with just the shock drive showed good consistency in spectral features and allowed us to divide out the incident spectrum. In Figure 2b, we can see some example spectra where background subtraction and correction for the incident spectrum have been performed.

The densities quoted in Figure 2b are derived from hydrodynamic simulation. For each shot, we carried out hydrodynamic simulations with the 1D HYADES code [13]. The experiment uses two-sided compression and so the aspect ratio of the shock width to target thickness is effectively >10 , justifying use of a 1D code. The code uses the SESAME equation of state database [14]. A typical case is shown in Figure 3a, where we can see that good uniformity in the direction normal to the shocks is expected. An important feature of shock compression experiments is that we do not vary the density independently of temperature. In Figure 3b, we show, for chlorinated parylene, how the density and temperature are strongly correlated for the shots taken. The dashed line is a linear fit that approximately describes the relationship between density and temperature. The error bars are based on combining the standard deviation for the 150 simulation cells representing

the chlorinated layer and the variation in average density and temperature resulting from varying the intensity by $\pm 10\%$ and the timing of the probe by ± 30 ps, based on the accuracy of the laser energy measurements and streak camera resolution. We note that data close to solid density correspond to early time probing, where the simulation predicts some X-ray pre-heating of the sample.

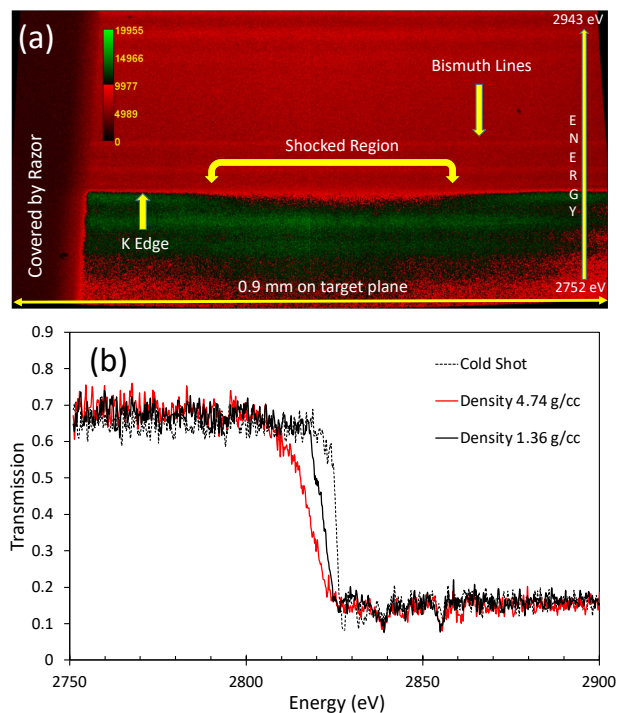


Figure 2. (a) Example of background-corrected Cl K-edge data. A point source projected through a shock-compressed chlorinated plastic sample, allowing spatial resolution across the shocked region in one direction. The colour scheme has been chosen to highlight the area of the shocked region. (b) Measured shifts for chlorinated plastic targets. The densities of the compressed cases are determined from hydrodynamic simulation.

In Figure 4, we see the measured edge positions as a function of the shocked density as derived from the hydrodynamic simulations. The error bars in edge position are derived from the resolution determined above. The Bi emission lines energies were taken from the literature. We took the absolute position of the cold K-edge (defined by the mid-point of the drop in transmission and available on each shot due to the spatial resolution) to be 2822.4 eV, in good agreement with previous work [4]. We note that establishing the cold edge from the positions of the known Bi emission lines leads to an edge position several eV higher than this, and outside values given in the literature. Hydrodynamic simulation, coupled with analysis using the FLYCHK code [15], was used to show that this is due to the Doppler shift observed in these lines due to motion of the source plasma (see Supplementary Material) and correcting for this gives agreement with the value taken to be better than the resolution of the experiment.

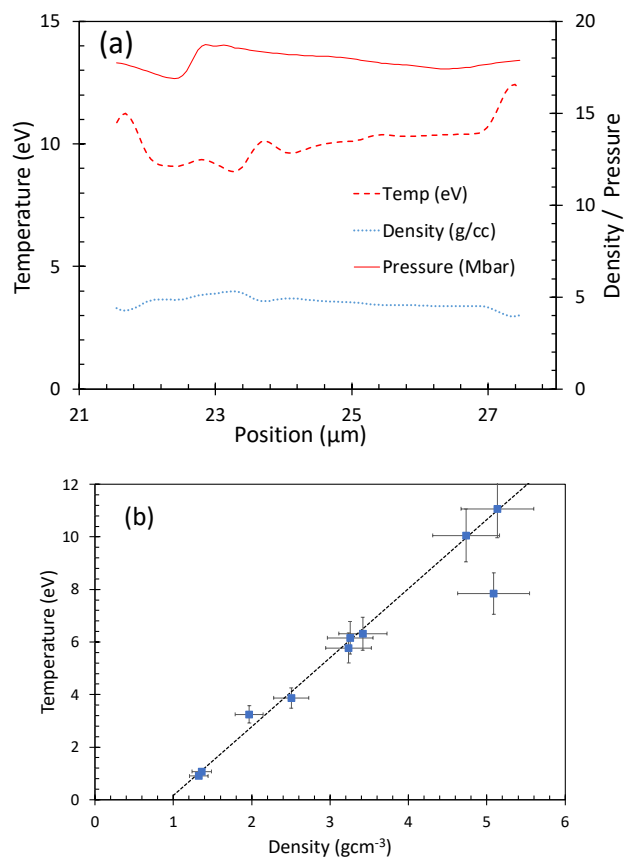


Figure 3. (a) Typical shock-compressed profile showing only the parylene-C part of the target, probed at 1.6 ns from the start of the shock drive pulse. (b) Relationship between simulated average density and simulated average temperature for the data shots taken in the experiment. We have averaged the conditions over the 200 ps of the probe duration.

The figure shows the calculated edge positions which we have modelled using two approaches to IPD. The first of these (solid blue line) is based on the treatment of Crowley (Equation (74) of [9]). This is similar to the Stewart–Pyatt model but allows for electron polarisation. In applying this treatment, we have derived separate average ionisations for H, C and Cl using the Thomas–Fermi (TF) mixture code of Shemyakin et al. [16]. This allows us to calculate an average ionisation, average perturber charge and the average ionisation of the test ions (Cl). In order to estimate the effect of having fractional average ionisations, we performed calculations, where instead of using the average ionisation of each element to calculate the necessary powers of the average ionisation state, we took each element to comprise a weighted mix of two adjacent ion stages. There was no difference within the resolution of the experiment in the predicted edge position. In order to obtain the spectral IPD, we need to account for the additional relaxation energy on ionising an electron from the K-edge to the continuum. This is derived from Equation (57) of Crowley [9], which is valid in the strong coupling limit, which is defined by

$$\Gamma = \frac{(Z^*e)^2}{4\pi\epsilon_0 R_i k_B T_i} \tag{1}$$

where $k_B T_i$, R_i and Z^* are the ion temperature, average ion sphere radius and average ionisation, respectively. The value is greater than 10 for all our cases. We also account for the degeneracy of the free electrons, which we do using the chemical potential. Note that we define the edge as the mid-point of the drop in transmission experimentally and so use this in the modelling. Our second approach (dashed red line) uses the equation of Ecker and Kröll [12], in the form given in [9] for the IPD. In Figure 4a, we compare the

measured edge positions to predictions where we scale the temperature used with density according to the predictions of the hydro-code simulations. In both cases, the ionisation state of Cl predicted from the Thomas–Fermi model [16] is used to give the edge shift due to ionisation. We can see that Crowley clearly gives a better fit overall. The Ecker–Kröll approach matches the data at the lowest density points but produces a much larger redshift than is seen experimentally for higher compressions. For the Ecker–Kröll approach, we rapidly get to the point that the IPD is greater than the outer shell ionisation energy for the ions and thus not consistent with the ionisation given by the Thomas–Fermi mixture code. The black dashed line in Figure 4a represents the calculation based on the IPD given by Stewart–Pyatt without the effect of electron polarisation (Equation (14) of Crowley). Finally, the dotted black line represents calculations using Equation (74) of Crowley where we have reduced the temperatures used by a factor of 2/3. This is relevant to the discussion of the DFT simulation results below. In Figure 4b, for reference, we present different components of the calculated shifts used in Figure 4a. As a first step in interpreting our results, we can state two things. First, the effect of electron polarisation is clearly not trivial and for these shock-compressed conditions, they should be accounted for. Secondly, the expected rapid increase in shift predicted using the Ecker–Kröll approach is clearly not matched in experiments, with a much more gentle variation seen that is more akin to the expected variation from the Stewart–Pyatt approach.

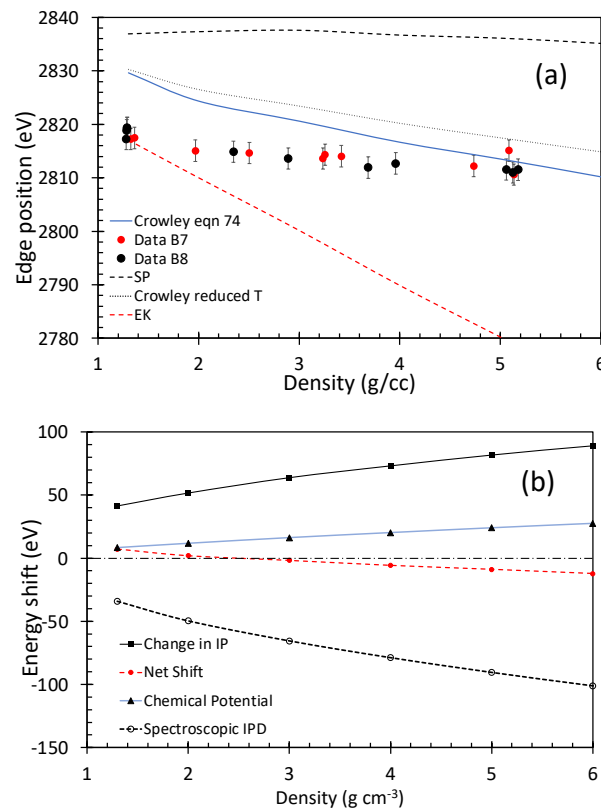


Figure 4. (a) Measured edge position for shocked Parylene-C. For the lowest density cases, probing was conducted before the shock reached the chlorinated layer but radiative pre-heating was predicted and small red-shifts were recorded. We compare the edge position with predictions using Equation (74) of the treatment of Crowley [9] (solid blue line) which is based on the Stewart–Pyatt model with the Ecker–Kröll model. The simulations are plotted against density but are not at a fixed temperature, see text for more details. The temperature is varied with the density according to the hydrodynamic simulations presented above. (b) Plot of the components contributing to the shifts in (a) using Crowley.

4. DFT Simulations

In Figure 5, we see the result of a DFT simulation for a typical case for the parylene-C targets. Using the temperature and density predicted by the hydrodynamic simulations, we can see the K-edge is predicted to be around 7 eV further red-shifted compared to experiment. In addition, we can see that the slope of the edge is predicted to be shallower. We can get a better fit to the data by assuming the hydrodynamic simulations overestimate the temperature. In Figure 5, we have fitted to a temperature that gives a good fit to the slope of the edge. We have varied the density within a range based on hydrodynamic modelling of the uncertainty in timing and laser energy. We see that the density has much less of an influence than temperature. In Figure 4a above, we have assumed a similar proportional reduction in temperature across all densities for the analytical model based on Crowley Equation (74). As we see, this predicts an upward shift in edge position but a similar variation with density.

Finally, we show in Figure 6 a comparison of the experimental data with a range of DFT simulations that were carried out under the density and temperature conditions predicted by HYADES. As we can see, the predicted shift varies with density in the same manner as the experimental data but with a more or less constant shift to lower energy. This indicates that a similar shift to lower temperature and slightly higher density, as carried out in Figure 5, would bring the DFT data into agreement with the experimental data across the density range.

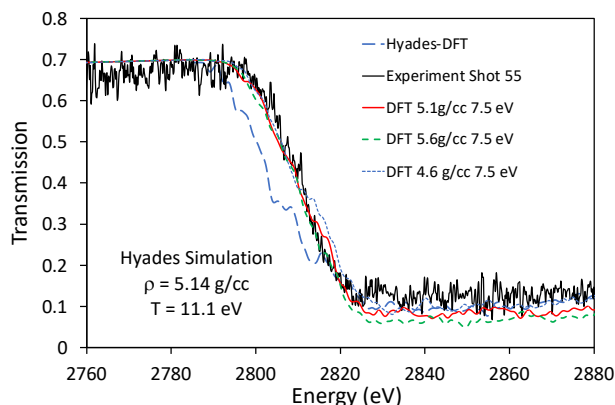


Figure 5. DFT simulations of K-edge for parylene-C in a high compression case.

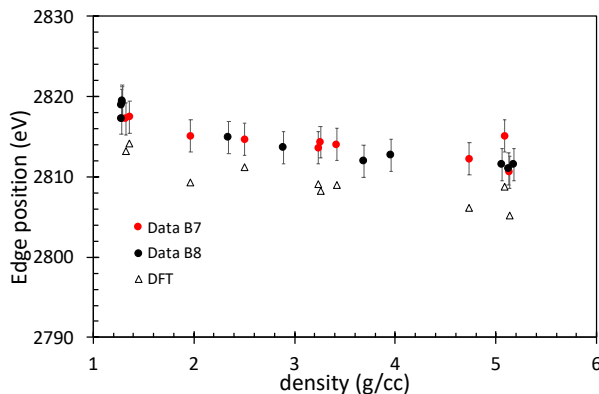


Figure 6. DFT simulations of K-edge position for parylene-C based on HYADES hydrodynamic data, compared to the experimental data.

5. Summary

In summary, our experiment, as we will mention below, has some limitations but does allow us to draw some useful conclusions. Firstly, our data do not show good agreement with modelling overall when the Ecker–Kröll model is used for the IPD. On the other

hand, it shows a better agreement with modelling when we use an approach similar to the Stewart–Pyatt model. Secondly, in achieving the better agreement, it was necessary to use the spectroscopic IPD, where we account for the change in interaction energy when an electron is photoionised from the K-shell and the effects of electron polarisation have been included.

In this work, we have relied upon hydrodynamic simulation to give us estimates of the density and temperature. These parameters, especially the latter, are difficult to measure in a direct way for warm dense matter. On the other hand, we have used a hydrodynamic simulation that has in the past been successful in reproducing, for example, expected shock speeds, which are of course tied to the density and temperature through the shock Hugoniot. With double-sided irradiation used to achieve high compression, it is not possible to implement an on-shot shock speed diagnostic. However, in further work, it would be useful to implement diagnostics to directly validate the HYADES code in situ with the same target materials but with one-sided irradiation. A separate Thomas–Fermi mixture model is used to calculate the ionisation for the edge shift calculations. This calculates the ionisation by taking the electron density at the boundary of the ion sphere for each element. There are refinements to the Thomas–Fermi model, such as exchange terms and gradient corrections and of course shell effects, which are not included. However, an arbitrary change in ionisation degree by $\pm 10\%$ was found to change the edge position by only $\pm 2\text{--}3$ eV for the simulated curve in Figure 4, not enough to alter our conclusions.

We have also used DFT molecular dynamics, which does not depend on the separation of free and bound electrons. Our results indicate that we can gain good agreement with the data but with a temperature lower than predicted by HYADES and by more than the expected variation due to laser energy measurement and probe timing. There are a couple of potential reasons for this. First, the shock pressure may not be as high as expected. However, this is governed by the absorption and transport of laser energy to the ablation front. The physics of this process have been well studied in recent decades and our laser conditions, with long pulses and moderate intensity, are in a well-studied regime. Another possibility is that the equation of state has an incorrect temperature. The pressure predicted for the Hyades simulation in Figure 5 of 5.14 g/cc and 11.1 eV is approximately 1300 GPa. This pressure would be reproduced at 7.5 eV for a density of 6 g/cc, only slightly outside the range of uncertainty we determined from the Hyades simulations. However, in the absence of reliable independent temperature and density diagnostics, this is a conclusion that would need to be followed up by further experiments.

Supplementary Materials: The following supporting information can be downloaded at: <https://www.mdpi.com/article/10.3390/atoms11100135/s1>, Figure S1: Chlorine H-alpha line group on spectrometer for dispersion calculation; Figure S2: Bismuth backlighter spectrum; Figure S3: Diagram of experimental arrangement for previous 2015 experiment; Figure S4: Hydrodynamic simulation of Bi in 2015 experiment; Figure S5: Hydrodynamic simulation of Bismuth in present experiment; Figure S6: FLYCHK simulation using Au as substitute for Bi for 2015 experiment conditions; Figure S7: FLYCHK simulation using Au as substitute for Bi for present experiment conditions. Related references [17–22] are cited in the supplementary materials.

Author Contributions: Conceptualization, D.R.; methodology, D.R. and S.W.; formal analysis, D.R., D.B., R.A.B. and S.P.D.M., supervision, D.R., S.P.D.M. and S.W., writing—original draft, D.R.; writing—review and editing, All authors; funding acquisition, D.R.; investigation, D.B., S.W., C.H., E.R.T., S.N.B., D.J.C., R.I., N.B., R.W. and B.K. All authors have read and agreed to the published version of the manuscript.

Funding: This work was supported by UK Engineering and Physical Sciences Research Council grant No. EP/K009591/1. B.K., R.A.B. and S.P.D.M. were supported by the European Research Council (ERC) under the European Union’s Horizon 2020 research and innovation programme (Grant Agreement No. 682399).

Data Availability Statement: Data used in this paper can be found on the QUB Pure website: doi: 0.17034/28535cb5-c85c-42fb-9cca-48e511a12519.

Conflicts of Interest: The authors declare no conflict of interest.

References

1. Lee, R.W.; Moon, S.J.; Chung, H.-K.; Rozmus, W.; Baldis, H.A.; Gregori, G.; Cauble, R.C.; Landen, O.L.; Wark, J.S.; Ng, A. Finite Temperature Dense Matter Studies on Next-Generation Light Sources. *J. Opt. Soc. Am. B* **2003**, *20*, 770–778. [[CrossRef](#)]
2. Graziani, F.; Desjarlais, M.P.; Redmer, R.; Trickey, S.B. (Eds.) *Frontiers and Challenges in Warm Dense Matter*, 1st ed.; Springer: Cham, Switzerland; Heidelberg, Germany; New York, NY, USA; Dordrecht, The Netherlands; London, UK, 2014.
3. Falk, K. Experimental methods for warm dense matter research. *High Power Laser Sci. Eng.* **2018**, *6*, e59. [[CrossRef](#)]
4. Bradley, D.K.; Kilkenny, J.; Rose, S.J.; Hares, J.D. Time-resolved continuum-edge-shift measurements in laser-shocked solids. *Phys. Rev. Lett.* **1987**, *59*, 2995–2998. [[CrossRef](#)] [[PubMed](#)]
5. DaSilva, L.; Ng, A.; Godwal, B.K.; Chiu, G.; Cottet, F.; Richardson, M.C.; Jaanimagi, P.A.; Lee, Y.T. Shock-induced shifts in the aluminum K photoabsorption edge. *Phys. Rev. Lett.* **1989**, *62*, 1623–1626. [[CrossRef](#)] [[PubMed](#)]
6. Riley, D.; Willi, O.; Rose, S.J.; Afshar-Rad, T. Blue Shift of the K Absorption Edge in Laser-Shocked Solids. *Europhys. Lett.* **1989**, *10*, 135–140. [[CrossRef](#)]
7. Ciricosta, O.; Vinko, S.M.; Chung, H.-K.; Cho, B.-I.; Brown, C. R. D. ; Burian, T.; Chalupský, J.; Engelhorn, K.; Falcone, R.W.; Graves, C; et al. Direct Measurements of the Ionization Potential Depression in a Dense Plasma. *Phys. Rev. Lett.* **2012**, *109*, 065002. [[CrossRef](#)] [[PubMed](#)]
8. Hoarty, D.J.; Allan, P.; James, S.F.; Brown, C.R.D.; Hobbs, L.M.R.; Hill, M.P.; Harris, J.W.O.; Morton, J.; Brookes, M.G.; Shepherd, R.; et al. Observations of the Effect of Ionization-Potential Depression in Hot Dense Plasma. *Phys. Rev. Lett.* **2013**, *110*, 265003. [[CrossRef](#)] [[PubMed](#)]
9. Crowley, B.J.B. Continuum lowering—A new perspective. *High Energy Density Phys.* **2014**, *13*, 84–102. [[CrossRef](#)]
10. Iglesias, C.A. A plea for a reexamination of ionization potential depression measurements. *High Energy Density Phys.* **2014**, *12*, 5–11. [[CrossRef](#)]
11. Stewart, J.C.; Pyatt, K.D. Lowering of Ionization Potentials in Plasmas. *Astrophys. J.* **1966**, *144*, 1203–1211. [[CrossRef](#)]
12. Ecker, G.; Kröll, W. Lowering of the Ionization Energy for a Plasma in Thermodynamic Equilibrium. *Phys. Fluids* **1963**, *6*, 62–69. [[CrossRef](#)]
13. Larsen, J.T.; Lane, S.M. HYADES-A plasma hydrodynamics code for dense plasma studies. *J. Quant. Spectrosc. Radiat. Transf.* **1994**, *51*, 179–186. [[CrossRef](#)]
14. Lyon, S.P.; Johnson, J.D. *Sesame: The Los Alamos National Laboratory Equation of State Database*; LANL Technical Report LA-UR-92-3407; Los Alamos National Laboratory: Los Alamos, NM, USA, 1992.
15. Chung, H.-K.; Chen, M.H.; Lee, R.W. Extension of atomic configuration sets of the Non-LTE model in the application to the K- α diagnostics of hot dense matter. *High Energy Density Phys.* **2007**, *3*, 57–64. [[CrossRef](#)]
16. Shemyakin, O.P.; Levashov, P.R.; Krasnova, P.A. Tfmix: A high-precision implementation of the finite-temperature Thomas–Fermi model for a mixture of atoms. *Comput. Phys. Commun.* **2019**, *235*, 378–387. [[CrossRef](#)]
17. Zhao, S.; Zhang, S.; Kang, W.; Li, Z.; Zhang, P.; He, X.-T. First-principles calculation of principal Hugoniot and K-shell X-ray absorption spectra for warm dense KCL. *Phys. Plasmas* **2015**, *6*, 062707. [[CrossRef](#)]
18. Trischka, J.W. Structure in the X-ray K Absorption Edges of Solid Potassium Chloride. *Phys. Rev.* **1945**, *11–12*, 318–320. [[CrossRef](#)]
19. Chung, H.K.; Chen, M.H.; Morgan, W.L.; Ralchenko, Y.; Lee, R.W. FLYCHK: Generalized population kinetics and spectral model for rapid spectroscopic analysis for all elements. *High Energy Density Phys.* **2005**, *1*, 3–12. [[CrossRef](#)]
20. Elliott, S.; Beiersdorfer, P.; Nilsen, J. Measurement of line overlap for resonant photopumping of transitions in neonlike ions by nickel-like ions. *Phys. Rev. A* **1993**, *2*, 1403–1406. [[CrossRef](#)] [[PubMed](#)]
21. Thompson, A.; Attwood, D.; Gullikson, E.; Howells, M.; Kwang-Je, K.; Kirz, J.; Kortright, J.; Lindau, I.; Liu, Y.; Pianetta, P.; et al. *X-ray Data Booklet*, 3rd ed.; Lawrence Berkeley National Laboratory: Berkeley, CA, USA, 2009.
22. Zhao, Y.; Yang, J.; Zhang, J.; Yang, G.; Wei, M.; Xiong, G.; Song, T.; Zhang, Z.; Bao, L.; Deng, B.; et al. K-shell photoabsorption edge of strongly coupled matter driven by laser-converted radiation. *Phys. Rev. Lett.* **2013**, *111*, 155003. [[CrossRef](#)] [[PubMed](#)]

Disclaimer/Publisher’s Note: The statements, opinions and data contained in all publications are solely those of the individual author(s) and contributor(s) and not of MDPI and/or the editor(s). MDPI and/or the editor(s) disclaim responsibility for any injury to people or property resulting from any ideas, methods, instructions or products referred to in the content.